74

SOCIETY OF AUTOMOTIVE ENGINEERS, INC.
Two Pennsylvania Plaza, New York, N. Y. 10001

Experimental and Theoretical Investigation of Turbulent Burning Model for Internal Combustion Engines

Norman C. Blizard and James C. Keck
Dept. of Mechanical Engineering, M. I. T.

SOCIETY OF AUTOMOTIVE ENGINEERS

Automotive Engineering Congress
Detroit, Mich.
February 25 - March 1, 1974

740191

740191

Experimental and Theoretical Investigation of Turbulent Burning Model for Internal Combustion Engines

Norman C. Blizard and James C. Keck
Dept. of Mechanical Engineering, M. I. T.

THE IMPOSITION of stringent emission standards for species such as nitric oxide (NO), carbon monoxide (CO), and hydrocarbons (HC) has required a greater understanding of the mechanisms that govern their formation in a spark-ignition (SI) (Otto) engine. Since rate-limited nonequilibrium reactions govern the formation and oxidation of such species, exhaust concentrations can only be calculated from precise measurements of pressure and attendant heat release as a function of crank angle. For example, digital calculation of time-resolved species concentrations by Heywood, et al., (1)* and Spadiccini and Chinitz (2) required knowledge of the pressure and temperature histories in the combustion chamber.

*Numbers in parentheses designate References at end of paper.

To determine the pressure and temperature histories from mathematical analysis, it is necessary to understand the mechanism of flame propagation. Specifically, in the turbulent combustion regime encountered in the majority of SI engines (3), a "burning law" correlation based upon the governing combustion equations would be of great utility in predicting the rate of energy release and pressure and temperature variations that in turn govern the reaction kinetics.

A survey of the relevant literature (1-8) indicates that at the present time no satisfactory burning law based upon fundamental principles exists, but empirical functionals of the form

$$x = x(\theta, \theta_s, \theta_d, \theta_b)$$

have been used to correlate experimental measurements. Here,

ABSTRACT

A model for describing turbulent flame propagation in internal combustion engines is presented. The model is based upon the assumption that eddies having a characteristic radius ℓ_e are entrained by the flame front at a turbulent entrainment velocity u_e and subsequently burn in a characteristic time $\tau = \ell_e/u_\ell$, where u_ℓ is the laminar flame speed for the fuel-air mixture. An approximate analytic method for determining the equilibrium state of the burned gases is also presented. To verify the predictions of the model, experiments were carried out in a single-cylinder research engine at speeds from 1000-3200 rpm, spark advances from 30-110 deg btc and fuel-air equivalence ratios from 0.7-1.5. Simultaneous measurements of the cylinder pressure and the position of the flame front as a function of crank angle were made, and good agreement with the predictions of the model was obtained for all operating conditions. Correlations were developed that permit both the entrainment speed u_e and the eddy radius ℓ_e to be calculated from a knowledge of the engine geometry, fuel type, and operating conditions. It is anticipated that the model will be useful for design studies directed toward improving the efficiency and pollution characteristics of internal combustion engines.

the dependent variable x is the mass fraction of gas burned, θ is the crank angle, θ_s is the ignition angle, θ_d is the induction angle or ignition delay, and θ_b is the apparent burning angle. The shortcomings of these empirical correlations are that they give little insight into the fundamental physics of the turbulent combustion process and cannot be used with any degree of confidence to extrapolate to conditions outside the bounds of measurements. Since this is frequently desirable in engine development programs, more reliable burning laws based upon models that embody the essential physics of the combustion process are clearly needed.

The purpose of this paper is to present an analysis in closed form that models the flame propagation mechanism based upon assumptions about the aerodynamics and chemistry in the combustion chamber. Quantitative verification of the internal consistency of the model will be made by experimental measurements.

The mathematical formulation of the model is given in the next section. The apparatus used in the experimental investigations is described, the experimental results are compared with the theoretical predictions, and a summary of the present work and some recommendations for future investigations are given.

GENERAL CONSIDERATIONS

TURBULENT COMBUSTION MODEL - Flame speeds in internal combustion engines have been observed to increase approximately linearly with engine speed (3). Increasing turbulent intensity with inlet Mach number is considered the mechanism for this behavior (9). Clark (10) and Semenov (11) have demonstrated that the jet nature of the intake process creates eddies or small-scale turbulence that persists during the combustion phase of the cycle.

If at ignition the assumption of a spatially homogeneous volume of persisting eddies is made, the combustion process can be viewed as the propagation of a flame front with finite thickness through the combustible mixture at a speed determined by the rate at which eddies are entrained u_e. In the proposed model, it is assumed that the entrained eddies are immediately ignited, due to diffusive transport of radicals such as H, OH, and O between adjacent eddies, and then burned at the laminar flame speed u_ℓ in a characteristic time

$$\tau = \ell_e / u_\ell \tag{1}$$

where ℓ_e is the characteristic eddy radius. From an aerodynamic view, the eddies burn as discrete microvolumes inwardly from the peripheral ignition sites. It is pointed out that this elementary approach incorporates the effects of engine speed, geometry, size, and spark advance in determining ℓ_e, whereas stoichiometry, fuel type, residual fraction, inlet mixture density, and spark advance determine u_ℓ. These effects are significant in engine design (12,13).

Following ignition, the expansion of the flame front proceeds at an accelerating rate due to the increase in the area of the flame front A_f and the density of the unburned gas ρ_u caused by the expansion of the burned gas. We assume, however, that the eddy entrainment speed u_e is a slowly varying parameter on the time scale of the combustion process. Under these conditions, the rate at which mass is entrained by the flame front is

$$M_f = \rho_u A_f u_e \tag{2}$$

If we further assume that the distribution of burning times for the entrained eddies is exponential, then the mass burned at a time t after ignition will be

$$M_b = \int_0^t (1 - e^{-(t - t')/\tau}) \rho_u A_f u_e dt' = M_f - \tau \dot{M}_b. \tag{3}$$

where

$$M_f = \int_0^t \rho_u A_f u_e dt' \tag{4}$$

is the total entrained mass and

$$\dot{M}_b = \int_0^t e^{-(t - t')/\tau} \rho_u A_f u_e dt'/\tau \tag{5}$$

is the mass burning rate. In Eq. 3, the factor $\rho_u A_f u_e dt'$ represents the mass entrained by the flame front in a time interval dt' at t' while the factor $(1 - e^{-(t - t')/\tau})$ is the mass fraction burned at a time $t - t'$ after entrainment. It should be noted that this exponential burning law has not been rigorously derived, but is introduced as a convenient analytic form that incorporates the basic features of turbulent combustion.

From purely thermodynamic considerations, Lavoie, Heywood, and Keck (6) have also derived an alternative expression for the burned mass.

$$M_b = \frac{pV - p_i V_i + (\gamma_b - 1)(W + Q) + (\gamma_b - \gamma_u) M c_{vu} (T_u - T_i)}{(\gamma_b - 1)(h_{fu} - h_{fb}) + (\gamma_b - \gamma_u) c_{vu} T_u} \tag{6}$$

where

$$M = \rho_i V_i = M_f + \rho_u (V - V_f) \tag{7}$$

is the total mass of gas in the combustion chamber,

$$W = \int_{V_i}^{V} p dV' \tag{8}$$

is the work done by the gas, and

where:

Q = heat lost by gas
p = pressure
T = temperature
V = volume of combustion chamber
V_f = volume enclosed by flame front
h_f = effective specific enthalpy of formation of gas mixture at absolute zero
c_v = effective specific heat at constant volume
$\gamma = c_p/c_v$ = ratio of specific heat
i, b, u = inlet conditions, burned, and unburned gases, respectively

Using the perfect gas law

$$p = \rho RT \tag{9}$$

and the relation

$$p/p_i = (\rho_u/\rho_i)^{\gamma_u} \tag{10}$$

for isentropic compression of the unburned gas mixture, we obtain from Eqs. 3-7

$$x = \int y(1 - e^{-(t - t')/\tau})(A_f u_e/V)\, dt' \tag{11}$$

$$x = [I + \epsilon y^{\gamma-1}(y - 1)]/[b_i (V/V_i)^{\gamma-1} - \epsilon y^{\gamma-1}] \tag{12}$$

and

$$V_f = V(y - 1 + x_b + \tau \dot{x}_b)/y \tag{13}$$

where

$$x = M_b/M \tag{14}$$

$$y = (V/V_i)(p/p_i)^{1/\gamma} \tag{15}$$

$$b_i = (h_{fu} - h_{fb})/c_{vu}T_i \tag{16}$$

$$\epsilon = (\gamma_u - \gamma_b)/(\gamma_b - 1) \tag{17}$$

$$\gamma = \gamma_u \tag{18}$$

$$I = \gamma V^{\gamma-1} \int_0^t (y/V)^{\gamma-1} \dot{y} dt' \tag{19}$$

Eqs. 11-13 constitute a set of three coupled integro-differential equations containing the four unknowns x, y, A_f, and V_f. To obtain a fourth equation to determinatively complete the set, the shape of the flame front must be determined. In general, this will be a very difficult problem involving consideration of the aerodynamics of the expanding fireball within the combustion chamber. However, for simple configurations where there is some degree of symmetry, reasonable approximations can often be found from geometrical considerations alone. Once the relation between A_f and V_f has been established, the full set of equations can be solved either by approximate analytic or numerical techniques, depending upon the value of the parameters u_e, τ, b_i, γ, and ϵ and the character of the function V(t).

SPHERICAL FLAME IN CYLINDER - To illustrate the application of the proposed technique and to obtain results which may be used to test the underlying physical assumptions of the combustion model, we shall consider a relatively simple case of particular interest in connection with automotive engines. The geometry is shown schematically in Fig. 1. The combustion chamber is a right circular cylinder of radius R and variable height.

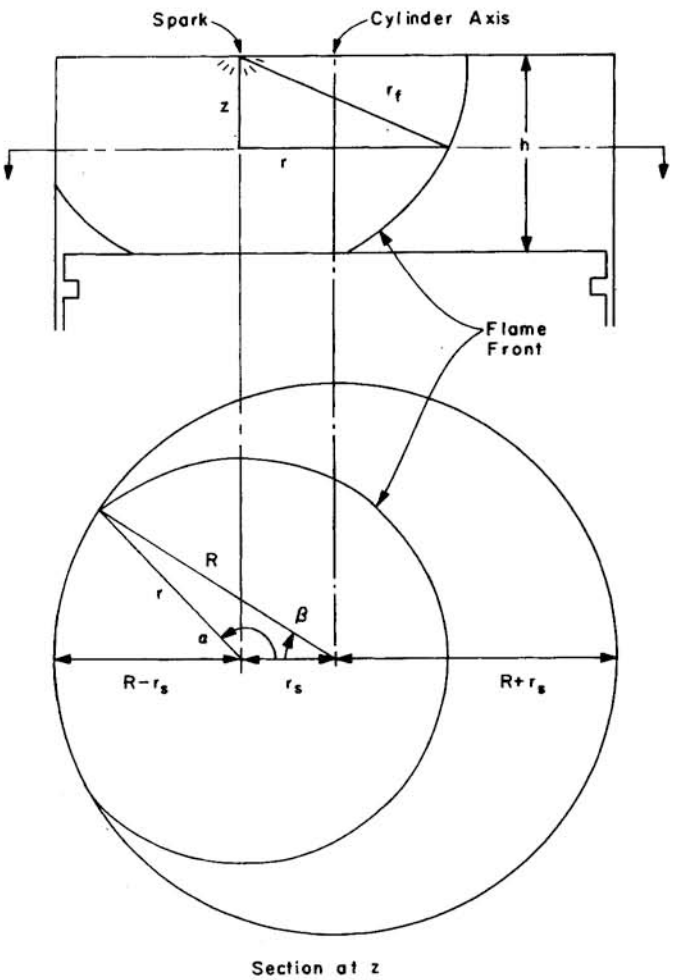

Fig. 1 - Schematic diagram of spherical flame front in cylinder

$$h = h_0 + \frac{1}{2} S (1 - \cos\theta), \tag{20}$$

where:

h_0 = clearance height
S = stroke
θ = crank angle relative to top center

As a first approximation, we shall assume that the flame spreads as a spherical wave from the point of ignition. Although aerodynamic effects due to swirl and nonuniform compression of the unburned gas ahead of the flame front will tend to modify this idealized behavior somewhat, it is anticipated that the effects will be relatively small for the geometry under consideration and will not introduce significant errors. It may also be noted in this connection that experimental observations for a wide range of conditions show an approximately spherical flame front.

Under these conditions, the area of the flame front and the enclosed volume are given by

$$A_f = 2r_f \int_0^h \alpha \, dz \tag{21}$$

and

$$V_f = \int_0^h (\alpha r^2 + \beta R^2 - r_s R \sin\beta) \, dz \tag{22}$$

where

$$\cos\alpha = (r_s^2 + r^2 - R^2)/2r_s r \tag{23}$$

$$\cos\beta = (r_s^2 + R^2 - r^2)/2r_s R \tag{24}$$

$$r^2 = r_f^2 - z^2 \tag{25}$$

and r_f is the radius of the flame front. Eqs. 21 and 22 may be easily integrated numerically and dimensionless plots of

$$a_f = A_f/2\pi R^2 \tag{26}$$

and

$$v_f = V_f/\pi R^2 h \tag{27}$$

as functions of

$$\tilde{r}_f = r_f/R \tag{28}$$

are shown in Fig. 2 for several values of

$$\tilde{h} = h/R \tag{29}$$

and a value of

$$\tilde{r}_s = r_s/R = .335 \tag{30}$$

corresponding to that for the engine used in the experimental investigations. It can be seen that for fixed $\tilde{h}$, a_f and v_f increase respectively as $\tilde{r}_f^2$ and $\tilde{r}_f^3$ until the flame front reaches either the piston face or the point on the side wall nearest to the spark. Thereafter, a_f goes through a broad maximum and then falls to zero at $\tilde{r}_f = \tilde{r}_m$, where

$$\tilde{r}_m = [(1 + \tilde{r}_s)^2 + \tilde{h}^2]^{1/2} \tag{31}$$

is the dimensionless distance from the spark to the point in the chamber farthest from the spark. At the same time, v_f continues to rise more or less linearly with $\tilde{r}_f$ until all the unburned gas has been entrained at $\tilde{r}_f = \tilde{r}_m$.

Eqs. 21 and 22 provide the relation between A_f and V_f necessary to complete the set of Eqs. 11-13. Accordingly, a first-order solution of these equations, which may be improved by iteration if required, can now be obtained as follows. We first observe that near peak pressure the cylinder volume

$$V = \pi R^2 h \tag{32}$$

will be a slowly varying function of time. We further anticipate that under most practical conditions the term $\tau\dot{x}_b$ in Eq. 13 will be negligible compared to y and that the turbulent entrainment speed u_e will be nearly constant. Eq. 19 may then be integrated and combined with Eqs. 11-13 to give

$$x = \left(\frac{2u_e}{\omega h}\right) \int_0^{\theta-\theta_s} a_f y (1 - e^{-(\theta-\theta_s-\theta')/\theta_\tau}) \, d\theta' \tag{33}$$

$$x = \frac{(1+\epsilon)(y^\gamma - 1) - \epsilon(y^{\gamma-1} - 1)}{b - \epsilon y^{\gamma-1}} \tag{34}$$

and

$$v_f = \frac{(b - \epsilon y^{\gamma-1})(y-1) + (1+\epsilon)(y^\gamma - 1) - \epsilon(y^{\gamma-1} - 1)}{y(b - \epsilon y^{\gamma-1})} \tag{35}$$

where

$$b = b_i (h/h_i)^{\gamma-1} \tag{36}$$

$$\theta = \omega t + \theta_s \tag{37}$$

$$\theta_\tau = \omega \tau \tag{38}$$

is the eddy burning angle, θ_s is the spark angle, and we have used the definitions of Eqs. 26, 27, and 32. We next observe that the value of v_f given by Eq. 35 can be well approximated by the expression

$$v_f = (1 - y^{-1})/(1 - y_1^{-1}) \tag{39}$$

where

$$y_1 = [(b_1 + 1)/(\epsilon + 1)]^{1/\gamma} \tag{40}$$

is the value of y for x = 1, that is, for the fully burned mixture. Finally, we assume that to first-order the radius of the flame front as a function of θ can be initially approximated by the expression

$$\tilde{r}_f^{(1)} \approx \left[\theta - \theta_s - \theta_d \left(1 - e^{-(\theta-\theta_s)/\theta_d}\right)\right] /\theta_b \tag{41}$$

where θ_d is an induction angle and θ_b is an apparent burning angle. Using Eqs. 26-29 and 39 and noting that for slowly varying $\tilde{h}$

$$a_f \approx \frac{\tilde{h}}{2}\left(\frac{dv_f}{d\tilde{r}_f}\right) \approx \frac{\tilde{h}}{2y^2(1 - y_1^{-1})}\left(\frac{dy}{d\tilde{r}_f}\right) \tag{42}$$

Eq. 33 can be integrated approximately to give

$$x^{(1)} \approx \frac{2}{15}\left(\frac{u_e}{\omega R}\right) \frac{\theta_b \theta_d (y - 1)}{\theta_\tau (1 - y_1^{-1})} \tag{43}$$

for $\theta - \theta_s < \theta_\tau \leq \theta_d$ and

$$x^{(1)} \approx \left(\frac{u_e}{\omega R}\right) \frac{\theta_b \ell n\, y}{(1 - y_1^{-1})} \tag{44}$$

for $\theta_\tau \leq \theta_d < \theta - \theta_s$. The value of θ_b can now be determined by requiring the values of x given by Eqs. 44 and 34 to match

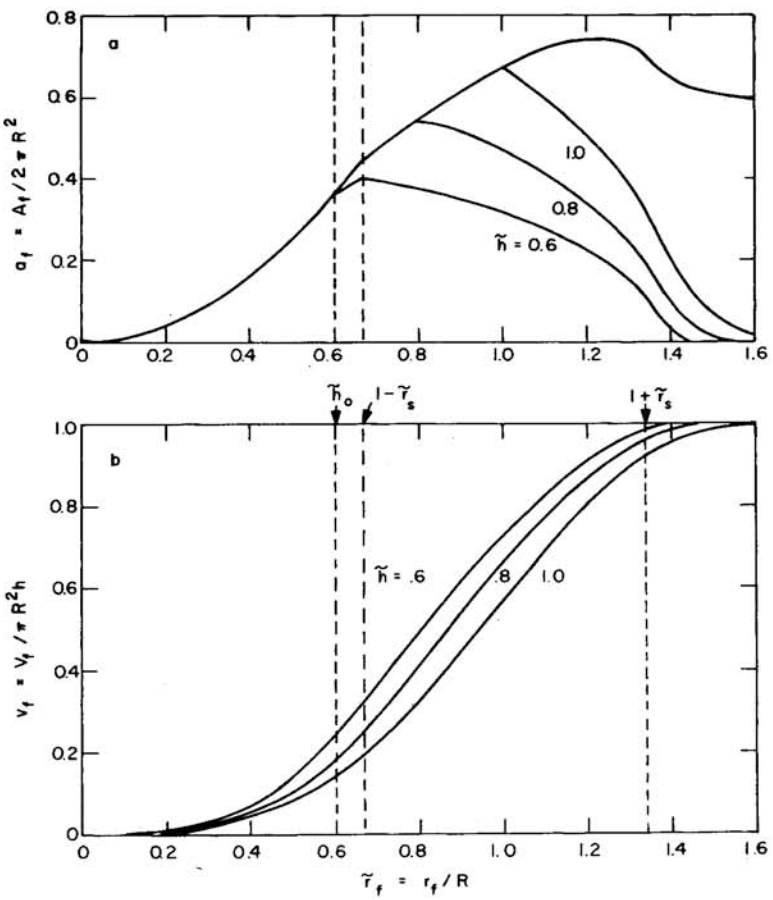

Fig. 2 - Dimensionless plots of flame front area a_f and fraction of cylinder volume enclosed by flame front v_f as functions of radius of flame front $\tilde{r}_f$ for several values of cylinder height $\tilde{h}$. For engine employed in experiments, radius of engine R = 1.25 in and dimensionless clearance height $\tilde{h}_b$ = 0.60 as shown. Discontinuities in derivative $da_f/d\tilde{r}_f$ occur at radii where flame front strikes either piston face $\tilde{r}_f = \tilde{h}$ or cylinder wall nearest spark $\tilde{r}_f = 1 - \tilde{r}_s = 0.67$

at the point $y = y_1$. This gives

$$\theta_b = \left(\frac{\omega R}{u_e}\right) \frac{(1 - y_1^{-1})}{\ell n\, y_1} \tag{45}$$

Similarly, the value of θ_d can be determined by requiring Eqs. 43 and 34 to match in the limit $y - 1 \ll 1$. This gives

$$\theta_d = \frac{15}{2} \left(\frac{\omega \ell_e}{u_\ell}\right) \left(\frac{\gamma + \epsilon}{b_s - \epsilon}\right) \ell n y_1 \tag{46}$$

in which we have used Eq. 1.

Having thus obtained a first-order solution for $\tilde{r}_f$ as a function of θ, the remaining first-order solutions for a_f, v_f, y, and x can easily be found from Fig. 2 and Eqs. 35 and 34. Although in principle, this solution can be improved by iteration, in cases where this was tried, the improvement was negligible, and it is anticipated that the first-order solution will be satisfactory for most practical applications.

SIMPLIFIED THERMODYNAMIC MODEL - To facilitate the calculation of the parameters b_i, γ, and ϵ, we have developed a simplified equilibrium thermodynamic combustion model. The model is valid in the temperature range $3000 < T < 5000$ R, and comparison of the results with those obtained from the more accurate thermodynamic calculations of Hottel, et al., (14) shows agreement within ±5%.

We shall consider the oxidation of a general hydrocarbon C_nH_m in a mixture of air and combustion products. We assume that the only thermodynamically important species are C_nH_m, N_2, O_2, H_2O, CO_2, CO, and H_2 and that the reaction is described by the chemical equation

$$(1 - \eta) \sum_{i=1}^{4} \nu_i X_i + \eta \sum_{i=2}^{7} \nu_i' X_i \longrightarrow \sum_{i=2}^{7} \nu_i' X_i \tag{47}$$

where X_i denotes a molecular species, ν_i and ν_i' are the corresponding stoichiometric coefficients for the unburned and burned gases, η is the mole fraction of burned gas recycled, and the subscripts i = 1 - 7 index the species C_nH_m - H_2 in the order given above.

Assuming for simplicity that the intake air is dry, we obtain for the fresh charge

$$\nu_1 = \phi \tag{48 HC}$$

$$\nu_2 = (79/21)n\,(1 + \mu/2) \tag{48 N_2}$$

$$\nu_3 = n(1 + \mu/2) \tag{48 O_2}$$

and

$$\nu_4 = 0 \tag{48 H_2O}$$

where ϕ is the equivalence reaction and

$$\mu = m/2n \tag{49}$$

The equations for conservation of atoms then give

$$(79/21)n\,(1 + \mu/2) = \nu_2' \tag{50 N}$$

$$2n\,(1 + \mu/2) = 2\,(\nu_3' + \nu_5') + \nu_4 + \nu_6 \tag{50 O}$$

$$n\phi = \nu_5' + \nu_6' \tag{50 C}$$

$$n\mu\phi = \nu_4' + \nu_7' \tag{50 H}$$

for N, O, C, and H, respectively. If we further assume that the overall water-gas reaction

$$H_2O + CO \longleftrightarrow CO_2 + H_2 \tag{51}$$

is in equilibrium, we obtain the additional relation

$$\nu_5'\,\nu_7'/\nu_4'\,\nu_6' = K(T) \tag{52}$$

where K(T) is the equilibrium constant for the reaction. Values of K(T) based on data from the JANAF tables (15) are given below

T(R) =	2700	3600	4500	5400
K(T) =	0.38	0.22	0.17	0.14

It can be seen that for the temperature range of interest K(T) is somewhat less than unity and varies relatively slowly.

The five equations Eqs. 50 and 52 contain the six unknowns $\nu_2' - \nu_7'$. To obtain a sixth equation, we make the approximation that for lean mixtures the concentration of H_2 is negligible; that is,

$$\nu_7' = 0 \text{ for } \phi \leqslant 1 \tag{53a}$$

while for rich mixtures the concentration of O_2 is negligible; that is,

$$\nu_3' = 0 \text{ for } \phi \geqslant 1 \tag{53b}$$

We may then solve to obtain for $\phi \leqslant 1$ (lean mixtures)

$$\nu_2' = 3.76\, n(1 + \mu/2) \tag{54 N_2}$$

$$\nu_3' = n(1 + \mu/2)\,(1 - \phi) \tag{54 O_2}$$

$$\nu_4' = n\mu\phi \tag{54 H_2O}$$

$$\nu'_5 = n\phi \qquad (54\ CO_2)$$

$$\nu'_6 = 0 \qquad (54\ CO)$$

$$\nu'_7 = 0 \qquad (54\ H_2)$$

and for $\phi \geqslant 1$ (rich mixtures)

$$\nu'_2 = 3.76n\,(1 + \mu/2) \qquad (55\ N_2)$$

$$\nu'_3 = 0 \qquad (55\ O_2)$$

$$\nu'_4 = n\mu\phi - \nu'_7 \qquad (55\ H_2O)$$

$$\nu'_5 = n\phi - \nu'_6 \qquad (55\ CO_2)$$

$$\nu'_6 = n(2 + \mu)\,(\phi - 1) - \nu'_7 \qquad (55\ CO)$$

$$\nu'_7 = n(B/2A)\,[\pm(1 + 4A^2/B)^{1/2} - 1] \qquad (55\ H_2)$$

where

$$A = \frac{\mu K\,(2 + \mu)\,\phi\,(\phi - 1)}{(1 + \mu K) - (1 + \mu)\,(1 - K)\,(\phi - 1)} \qquad (56a)$$

$$B = \frac{\mu K\,(2 + \mu)\,\phi\,(\phi - 1)}{(1 - K)} \qquad (56b)$$

Note that for $K < 1$, which is the case of interest, A has a singularity at

$$\phi^* = 1 + (1 + \mu K)/(1 + \mu)\,(1 - K) \qquad (57)$$

where, from Eq. 55 H_2,

$$\nu'_7\,(\phi^*) = n\sqrt{B^*} \qquad (58)$$

For $\phi < \phi^*$, $A > 0$ and the plus sign applies in Eq. 55 H_2, while for $\phi > \phi^*$, $A < 0$ and the minus sign applies.

Using Eqs. 48, 54, and 55, the internal energy and number of moles of gas for the burned and unburned mixtures per mole of air can be determined. For the unburned mixture we find

$$e_u = e_{uc} + \eta(e_b - e_{uc}) + (\phi - 1)\,(1 - \eta)\,(e_{uc} - e_a) \qquad (59)$$

$$n_u = 1 + f_c + \eta(\eta_b - 1 - f_c) + (\phi - 1)\,(1 - \eta)\,f_c \qquad (60)$$

where

$$f_c = 0.42/n(\mu + 2) \qquad (61)$$

is the number of moles of fuel per mole of air for a stoichiometrically correct fuel-air mixture,

$$e_{uc} = f_c e_1 + e_a \qquad (62)$$

is the energy per mole of air for the correct unburned mixture

$$e_a = 0.79\,e_2 + 0.21\,e_3 \qquad (63)$$

is the energy per mole for air, and e_i is the energy per mole for the species i. For the burned mixture, we find for $\phi \leqslant 1$

$$e_b = e_{bc} + (\phi - 1)\,(e_{bc} - e_a) \qquad (64)$$

$$n_b = 1 + 0.21\mu/(\mu + 2) + 0.21\,(\phi - 1)\mu/(\mu + 2) \qquad (65)$$

and for $\phi \geqslant 1$

$$e_b = e_{bc} + (\phi - 1)(e_{bc} - e_a + .21\,\Delta e_1) - .42\nu'_7\Delta e_2/n(\mu + 2) \qquad (66)$$

$$n_b = 1 + 0.21\mu/(\mu + 2) + 0.42\,(\phi - 1)\,(\mu + 1)/(\mu + 2) \qquad (67)$$

where

$$e_{bc} = 0.79e_2 + 0.42\,(\mu e_4 + e_5)/(\mu + 2) \qquad (68)$$

is the energy of the burned gas per mole of air for a correct mixture,

$$\Delta e_1 = 2e_6 + e_3 - 2e_5 \qquad (69)$$

is the energy change in the reaction

$$2CO + O_2 \longrightarrow 2\,CO_2 \qquad (70)$$

per mole of O_2, and

$$\Delta e_2 = e_4 + e_6 - e_5 - e_7 \qquad (71)$$

is the energy change for the Eq. 51 per mole of CO.

Plots of e_{uc} and e_{bc} based upon data taken from Taylor and Taylor (16) are shown in Fig. 3 for a correct octane-air mixture at a density of 0.25 lb/ft^3. These curves are valid within a few percent for all common fuel hydrocarbons (except H_2 and C_2H_2) containing only H and C. Over the temperature and density range of interest for automotive engines, they may be approximated within a few percent by the expressions

$$e_{uc} \approx 34{,}200 + 6.0T \qquad (72)$$

and

$$e_{bc} \approx -15{,}800 + 10.7T \qquad (73)$$

where e is in Btu/lb mole air and T is in R.

Values of e_a, Δe_1, and Δe_2 based upon data taken from the JANAF tables are given in Table 1.

For the unburned gas, a good approximation is

$$e_{au} \approx -3200 + 5.5T \tag{74}$$

and for the burned gas, good approximations are

$$e_{ab} \approx -6200 + 6.8T \tag{75}$$

$$\Delta e_1 \approx 238{,}000 \text{ Btu/lb mole } O_2 \tag{76}$$

$$\Delta e_2 \approx 10{,}000 \text{ Btu/lb mole CO} \tag{77}$$

Substituting Eqs. 72-77 into Eqs. 59-61 and 64-67 and using the definition

$$c_v = (\partial e/\partial T)_v \tag{78}$$

we find for $\phi \leq 1$ (lean mixtures)

$$h_{fu} - h_{fb} = 50{,}000\,(1 - \eta)\phi \tag{79a}$$

$$c_{vu} = 6.0 + 0.5(\phi - 1) \tag{79b}$$

Table 1 - Internal Energy of Air e_a and Heats of Reaction Δe_1 and Δe_2 for $2CO + O_2 \rightarrow 2CO_2$ and $H_2O + CO \rightarrow CO_2 + H_2$ (15)

T, °R	e_a, Btu/lb mole	Δe_1, Btu/lb mole O_2	Δe_2, Btu/lb mole CO
560	0		
1080	2,800		
1800	6,800		
2700	12,200	241,800	12,900
3600	18,300	239,500	11,200
4500	24,400	237,300	9,700
5400	30,600	235,200	8,400

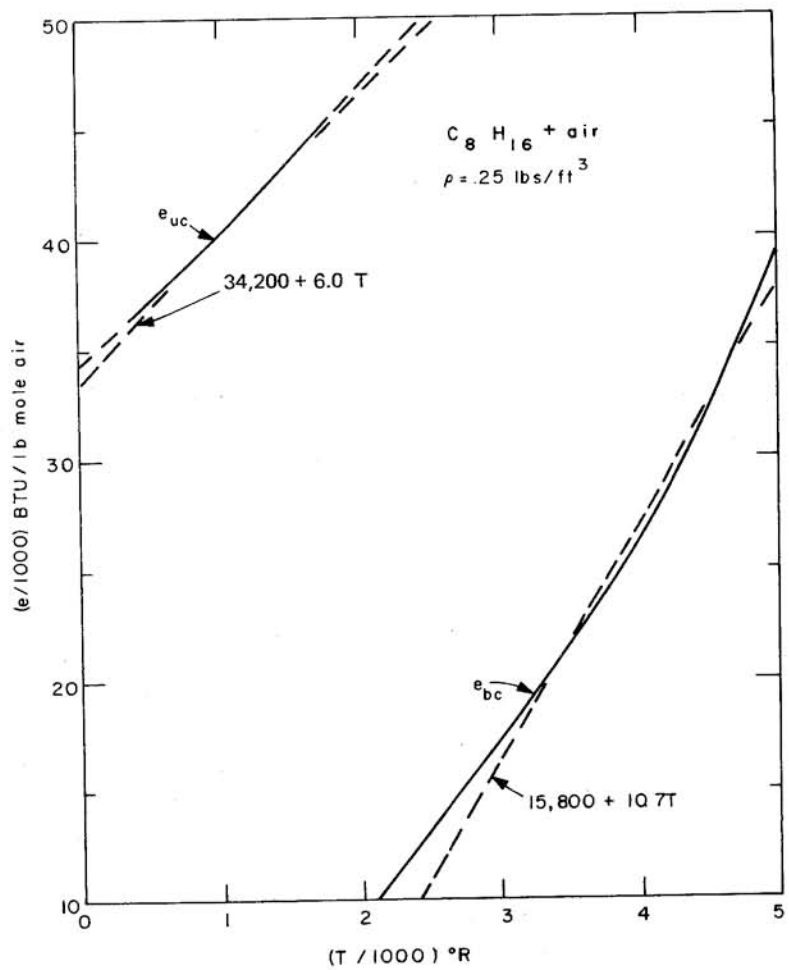

Fig. 3 - Solid curves show internal energies e_{bc} and e_{uc} of burned and unburned gases in Btu/lb mole of air for stoichiometrically correct octane/air mixtures at density of 0.25 lb/ft^3 as given by Taylor and Taylor (16). Dark lines show constant specific heat approximations used in present analysis. For temperature and pressure ranges of interest for automotive engines, curves are valid to few percent for all common fuels (except H_2 and C_2H_2) containing only H and C

$$c_{vb} = 10.7 + 3.9(\phi - 1) \quad (79c)$$

$$n_u = 1.02 + 0.05\eta + (0.02 + 0.05\eta)(\phi - 1) \quad (79d)$$

$$n_b = 1.07 + 0.07(\phi - 1) \quad (79e)$$

and for $1 \leqslant \phi \leqslant 1.8$ (rich mixtures to flammability limit)

$$h_{fu} - h_{fb} = 50{,}000\,(1 - \eta) \quad (80a)$$

$$c_{vu} = 6.0 + 0.5\,(\phi - 1) \quad (80b)$$

$$c_{vb} = 10.7 + 3.9\,(\phi - 1) \quad (80c)$$

$$n_u = 1.02 + 0.05\eta + (0.02 + 0.26\eta)(\phi - 1) \quad (80d)$$

$$n_b = 1.07 + 0.28\,(\phi - 1) \quad (80e)$$

where we have set $\mu = 1$ and n = 8 and neglected the small term $\nu'_7 \Delta e_2$ in Eq. 66 and the small difference between the heat capacities of unburned gas and cold (recycled) burned gas. Finally, combining Eqs. 79 and 80 with Eqs. 16-18, we find for an inlet temperature $T_i = 650$ R for $\phi \leqslant 1$,

$$b_i = 12.8\,(1 - \eta)\phi/[1 + 0.08\,(\phi - 1)] \quad (81a)$$

$$\gamma = 1 + 0.34\,[1 + 0.05\eta - (0.06 - 0.05\eta)(\phi - 1)] \quad (81b)$$

$$\epsilon = 1 - 1.70\,[1 + 0.05\eta + (0.23 + 0.06\eta)(\phi - 1)] \quad (81c)$$

and for $\phi \geqslant 1$

$$b_i = 12.8\,(1 - \eta)/[1 + 0.08\,(\phi - 1)] \quad (82a)$$

$$\gamma = 1 + 0.34\,[1 + 0.05\eta - (0.06 - 0.26\eta)\,(\phi - 1)] \quad (82b)$$

$$\epsilon = 1 - 1.70\,[1 + 0.05\eta + (0.04 + 0.26\eta)\,(\phi - 1)] \quad (82c)$$

Thus, the above described Eqs. 81-82 are provided to facilitate the calculation of the parameters b_i, γ, and ϵ for use in quantitative solutions of Eqs. 11-13 et. seq.

EXPERIMENTAL APPARATUS

DESCRIPTION OF ENGINE - A major consideration in implementing the experimental program to test the combustion model described in the preceding section was the requirement for a quiescent (nonswirl) cylindrical combustion chamber with nearly central ignition. The engine chosen was the smallest of M.I.T.'s geometrically similar engine (GSE) with the desirable feature of an easily serviceable head. The relevant specifications for this engine and the range of operating conditions investigated are summarized in Table 2.

The experimental installation was typical for a research engine. Torque was absorbed by an eddy current dynamometer as a measure of horsepower for redundant mep calculations. Fuel flow was obtained from a series rotometer that was calibrated by parallel burettes, and airflow was determined by the pressure drop across an ASME sharp-edged orifice. Homogeneity of the fuel-air mixture was ensured by injecting the fuel into a large steam-heated vaporizing tank. Cooling water was maintained at 180°F. Ignition timing was controlled by breaker points (dwell ≈ 60 deg) driven by the camshaft, and ignition was provided by a contemporary primary-secondary coil charged with a 120 V chopped d-c source. Crank angle was obtained from an optically chopped light emitting diode (LED) and photodiode jig, with appropriate signal shaping to generate 10 deg markers with a pedestal at tdc. A Beckman flame ionization detector was used to measure the HC concentration in the exhaust and a Beckman Model 15A nondispersive Infrared Analyzer was used to measure the CO and CO_2 concentrations. The equivalence ratio ϕ was determined both from the measured fuel and airflow rates and the measured carbon concentration in the exhaust. Dynamic pressure was measured by a Kistler 603A piezoelectric transducer calibrated by comparison with balanced pressure indicator (17) cards.

IONIZATION PROBES - The position of the flame front as a function of crank angle was measured using ionization probes. These have been used since 1934 with great success for detecting flame proximity (18-24). Calcote (25-27) has shown that the orders of magnitude increase in carbon ions during combustion of HC fuels gives rise to a similar increase in conductivity of the reacting gas. By this mechanism, both the arrival and degree of reaction relaxation at a given station can be measured as functions of time, using the gas as a variable resistance in a detection circuit.

Many abortive attempts at designing microminiature probes of sufficient durability were made before the present design was adopted. The configuration is part of an overall head design compatible with the GSE and is illustrated in Fig. 4. Probes consist of two subassemblies: a removable inner core

Table 2 - Summary of Engine Parameters and Operating Conditions

Engine speed, rpm	N	1000, 2100, 3200
Spark advance, deg btc	$-\theta_s$	30-110
Equivalence ratio	ϕ	0.8-1.6
Fuel		isooctane, C_8H_{18}
Inlet temperature, °F	T_i	190
Water temperature, °F	T_w	180
Oil temperature, °F	T_{oil}	140
Bore, in	b	2.5
Stroke, in	S	3.0
Clearance height, in	h_o	0.75
Inlet port diameter, in	D	0.98
Valve lift, in	L	0.19
Compression ratio	r_c	5.0
Intake manifold		WOT

and the water jacket well, which is electron beam welded to the aluminum head. The materials for head and well have the same coefficient of thermal expansion to obviate thermal strain failure at the weld, which had been a prior problem. Ends of the well are tapped for different reasons: the top is tapped to accept a coaxial connector while the bottom (combustion chamber) resists deposit fouling. The inner core consists of three components: a commercially obtainable miniature coaxial connector (Microdot Lepracon feed-through), center wire of 0.032 in diameter nickel welded to the connector, and a commercially available ceramic protection tube (Omega Eng. Co.) to insulate the center wire from the well. An O-ring seals the inner core assembly when installed. Inevitable fouling of the probes was not a problem because when loss of signal was observed, new probe cores were easily substituted without disturbing the head. Spatial resolution is estimated at twice the center wire height, or about 0.12 in. Unfortunately, this sensitivity is at least an order of magnitude larger than the estimated eddy size, so that direct observation from signal fluctuations was not possible. Attempts at using smaller center wires to improve the resolution were unsuccessful.

Five stations in the combustion chamber were selected for probe sites as a compromise between spatial resolution and physical limitations. Fig. 5 shows a photograph of the engine head. Fig. 6 shows the relation of the probe sites to the spark plug well and intake and exhaust valves schematically. Three probes (C-E) are symmetrically located at the periphery of the

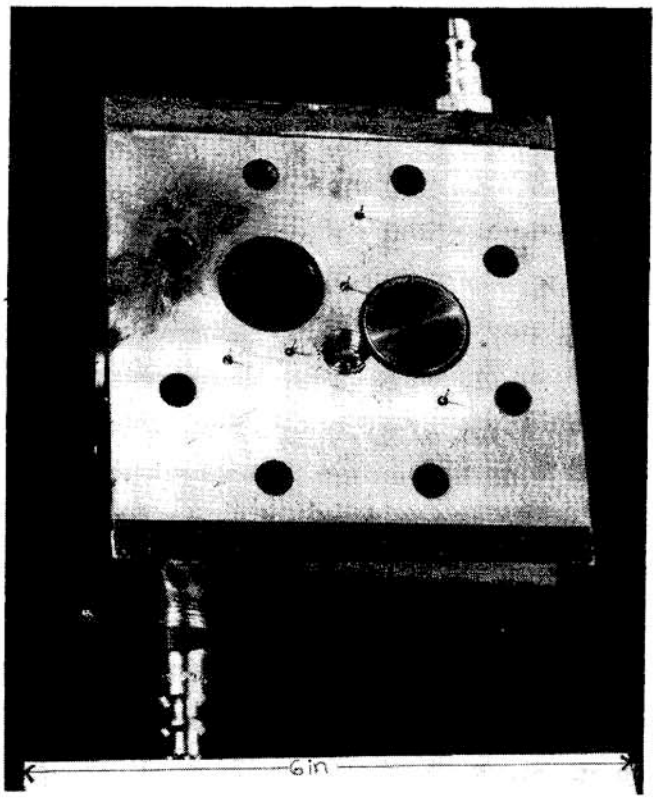

Fig. 5 - Cylinder head showing locations of ionization probes, spark plug, and valves

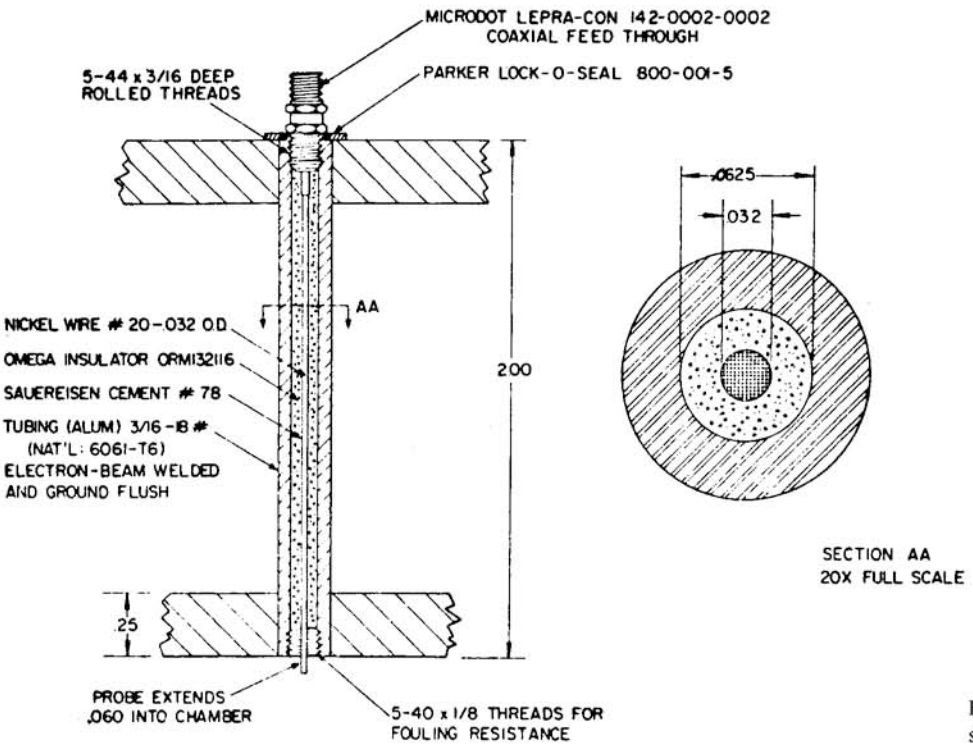

Fig. 4 - Schematic diagrams showing construction of ionization probes, in

combustion chamber, and two (A and B) are at approximately half the chamber radius. The spark plug site S is noncentral by about 30%.

Conductivity changes of the reacting gases in proximity with a biased probe were measurable as perturbations in the d-c voltage of the circuit illustrated in Fig. 7. A d-c bias (22-1/2 V battery) is applied to the probe across an a-c shunt capacitance. The voltage signal was measured at nodes V_s for the multiplexed arrangement shown. Using the specified line capacitance of the coaxial cable to the probes (UG 186/A having 29 pF/ft), we estimate the circuit time constant as 10 μs with a series resistance of 20 kΩ. Miniature coaxial terminations and connectors (Microdot) were used throughout and continuously monitored with pulsed test signals to ensure circuit integrity.

OSCILLOSCOPE DISPLAY - A Textronic Model 565 oscilloscope triggered by the spark was used to record the ionization probe signals, cylinder pressure, and crank angle. A typical display traced from a Polaroid photograph is reproduced in Fig. 8 for an engine speed N = 2100 rpm, spark advance $-\theta_s$ = 60 deg and equivalence ratio ϕ = 1.2. The four upper curves show the ionization probe signals; the two lower curves show the cylinder pressure and the 10 deg timing markers. It can be seen that the rise time of the ionization signals is about 0.2 ms, which agrees well with the resolution time of the probes based upon an estimated spacial resolution of 0.120 in and a flame speed of 0.5 in/ms at 2100 rpm. Following the initial rise, the signals fluctuate in a random manner, giving an indication of turbulent flame structure, and finally decay to zero in a time of a few milliseconds, which is long compared to the estimated time of 10^{-7} s for attachment of the electron to H_2O (28). This implies that the duration of the ionization signals is controlled by the thickness of the turbulent reaction zone. Although it had originally been anticipated that the ionization signals might give a direct measurement of the characteristic eddy size ℓ_e and burning time τ, the relatively low spacial resolution of the probes combined with mathematical difficulties in determining the mean flow field behind the flame front made such measurements too uncertain to be quantitatively useful. The probe signals were therefore used primarily to determine the flame speed and only secondarily as an internal consistency check on the values of ℓ_e and τ determined by the method described in the following section.

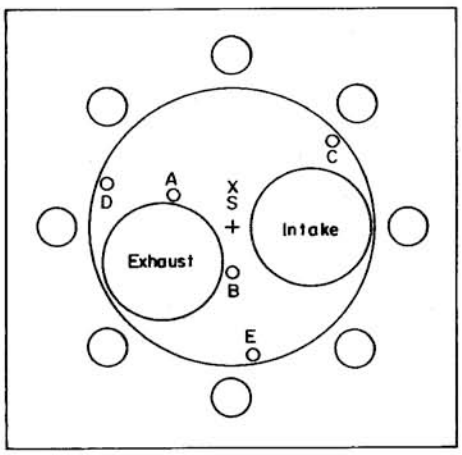

Cylinder Radius R = 1.25 in.

Spark Radius r_s = .42 in.

Probe Radii

A	B	C	D	E	
.60	.40	1.18	1.18	1.18	in.

Spark to Probe Distances

A	B	C	D	E	
.53	.82	.96	1.11	1.60	in.

Fig. 6 - Schematic of cylinder head showing location of ionization probes A–E and spark plug S

RESULTS AND CORRELATIONS

RESULTS - The experimental and theoretical results are compared in Figs. 9-13. The points show the experimental data and the estimated standard deviations; the curves are a "best fit" of the model to the data obtained using the correlations derived in the following section.

A log-log plot of the pressure as a function of cylinder volume is shown for a "motored" engine in Fig. 9 for N = 2100 rpm and ϕ = 1.0. The specific heat ratio for the unburned gas obtained from the slope of the line through the points is γ = 1.35, in excellent agreement with the theoretical value given by Eqs. 81b and 82b, and the corresponding inlet pressure is p_i = 11.2 psia. Combining these values with the cylinder volume V_i = 18.4 in^3, we find $p_i V_i^{\gamma}$ = 571 psia.

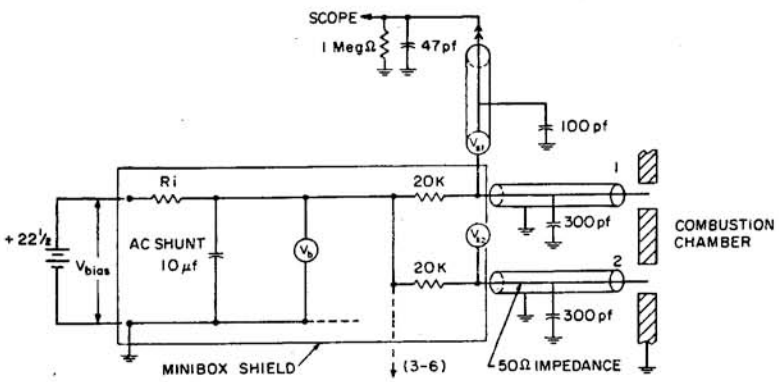

Fig. 7 - Schematic diagram of ionization probe circuit. Rise time of circuits determined by 20K load resistors and 400 pf cable capacities was approximately 10 μs. This is negligible compared to estimated time of 200 μs required for flame front to traverse active region of probes

Fig. 10 shows the mass fraction of burned gas x and the corresponding dimensionless flame radius $\tilde{r}_f$ a function of crank angle θ for N = 2100 rpm, $\phi = 1.0$, and $\theta_s = -30, -60$, and -110 deg. Also shown by the dashed curves are the radius $\tilde{r}_f = \tilde{h}$ at which the flame front strikes the piston face and the locus $v_f = 1$ at which the unburned gas is fully entrained. Finally, the arrows on the ordinate $\tilde{r}_f$ give the distances $1 - \tilde{r}_s$ and $1 + \tilde{r}_s$ from the spark plug to the near and far cylinder walls. Note that for $b >> \epsilon$, Eq. 34 gives to a good approximation $x \approx (y^\gamma - 1)/(y_1^\gamma - 1)$, where $y = pV^\gamma$ and y_1 is given by Eq. 40. It can be seen that following ignition, x rises very slowly at first approximately as $(\theta - \theta_s)^6$. $\tilde{r}_f$, on the other hand, rises relatively rapidly approximately as $(\theta - \theta_s)^2$. The theoretical curves reproduce this behavior quite well. Later, as $\tilde{r}_f$ approaches its maximum value given by the curve $v_f = 1$, the theoretical values of x approach unity while the experimental values go through a maximum and then decrease slowly. This is attributed to the effect of heat losses that were not included in the present model. The rate of the heat loss implied by the experimental data is approximately 0.2%/deg, which is reasonable near-peak pressure. It should be pointed out that in the theory as presented, it has been tacitly assumed that the value of the burning time τ tends to zero as x approaches unity due to the rapid increase in the laminar flame speed with the temperature of the adiabatically compressed unburned gas. If this were not the case, there would be a substantial increase in y^γ following complete entrainment of the unburned gas and this is not observed.

Fig. 11 shows the observed maximum values of y^γ as a function of the equivalence ratio ϕ for N = 2100 rpm and $\theta_s = -50$ deg. The curve labeled y_1^γ is the theoretical value of y^γ for the fully burned mixture calculated from Eqs. 40, 81, and 82. Because of the heat losses discussed in connection with

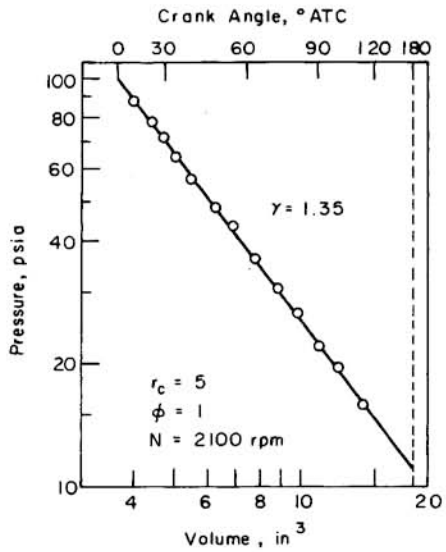

Fig. 9 - Log-log plot of pressure as function of volume for motored engine (no ignition) at 2100 rpm and $\phi = 1$. Slope of line gives value of $\gamma = 1.35$ for unburned mixture

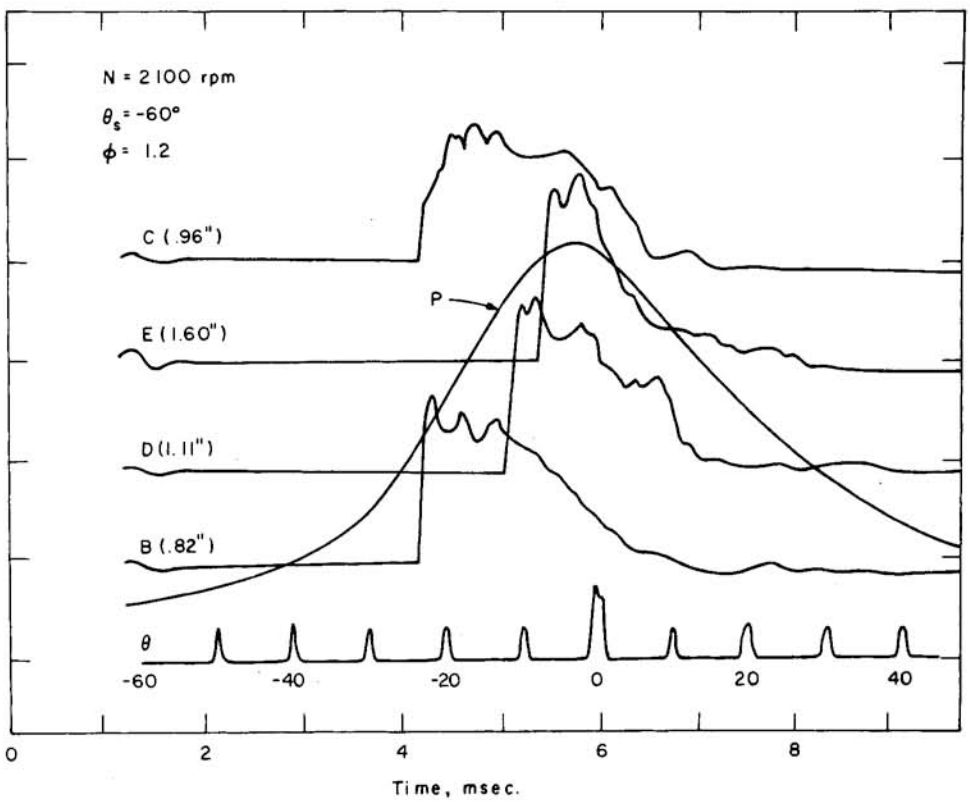

Fig. 8 - Tracing of typical oscillogram showing 10 deg crank angle θ markers, cylinder pressure p, and four of five ionization probe signals. Numbers in parentheses give spark to probe distances

Fig. 10, the values of y_m^γ are about 5% less than the predicted values of y_1^γ, which is quite acceptable.

Fig. 12 shows the crank angles $\theta_A - \theta_s$ and $\theta_E - \theta_A$ required for the flame front to travel from the spark plug to probe A and from probe A to probe E as a function of the equivalence ratio ϕ for N = 2100 rpm and $\theta_s = -50$ deg. These angles are also shown in Fig. 13 as a function of the spark advance $-\theta_s$ for $\phi = 1$ and N = 1000, 2100, and 3200 rpm. It can be seen in Fig. 12 that $\theta_A - \theta_s$ and $\theta_E - \theta_A$ have minima in the neighborhood of $\phi = 1$. In Fig. 13, it can be seen that $\theta_A - \theta_s$ and $\theta_E - \theta_A$ are increasing functions of engine speed and spark advance. This behavior is predicted by the theoretical curves calculated from Eq. 41. Note that $\theta_A - \theta_s$ is determined primarily by the induction angle θ_d, while $\theta_E - \theta_A$ is determined primarily by the apparent burning angle θ_b.

CORRELATIONS FOR u_e AND ℓ_e - To determine the fundamental parameters u_e and ℓ_e from the experimental data, a knowledge of the laminar flame speed u_ℓ is required. Simple theoretical considerations (29, 30) suggest this should have the functional form

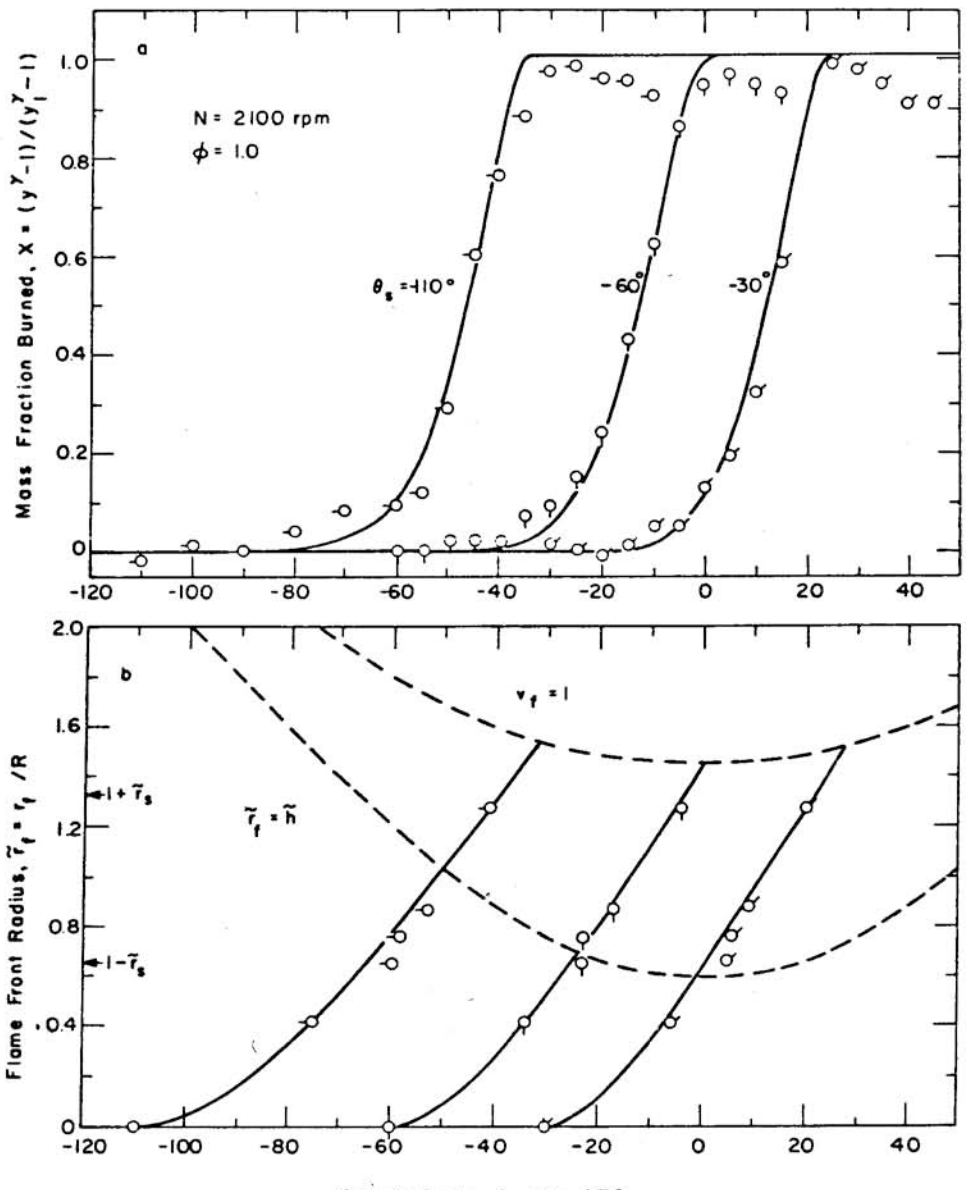

Fig. 10 - Mass fraction of burned gas x and dimensionless flame radius $\tilde{r}_f$ as functions of crank angle θ for equivalence ratio $\phi = 1$, engine speed N = 2100 rpm, and spark advances $-\theta_s$ = 30, 60, and 110 deg. Solid curves are best fit of theory to experimental points. Dashed curve labeled $\tilde{r}_f = \tilde{h}$ shows locus at which all unburned gas has been entrained by flame front. Also shown by arrows on ordinate of part b are dimensionless distances $1 - \tilde{r}_s$ and $1 + \tilde{r}_s$ from spark plug to near and far cylinder walls. Note that to a good approximation, $x \approx (y^\gamma - 1)/(y_1^\gamma - 1)$ where $y^\gamma = pV^\gamma/p_1V_1^\gamma$

$$u_\ell = u_0 \left(\frac{\rho_0}{\rho_u}\right)^{\alpha} \exp \frac{E_A}{2R} \left(\frac{1}{T_{b0}} - \frac{1}{T_b}\right) \qquad (83)$$

where:

E_A = apparent activation energy

α = exponent determined by order of combustion reaction

u_0 = flame speed for reference condition $T_b/T_{b0} = \rho_u/\rho_0 = 1$

For isenthalpic combustion, the burned gas temperature is given by

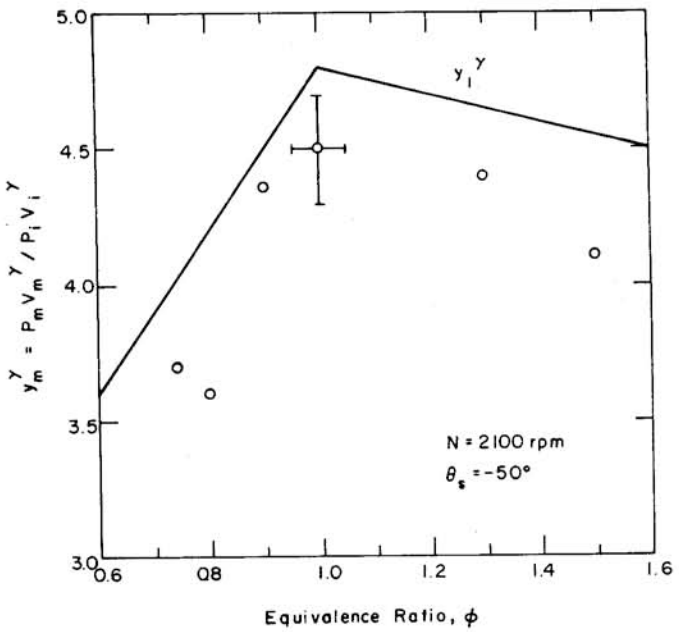

Fig. 11 - Maximum value of $y^\gamma = pV^\gamma/p_iV_i^\gamma$ as function of equivalence ratio ϕ for N = 2100 rpm and θ_s = −50 deg. Curve gives theoretical value y_1^γ for fully burned gas in absence of heat or mass loss

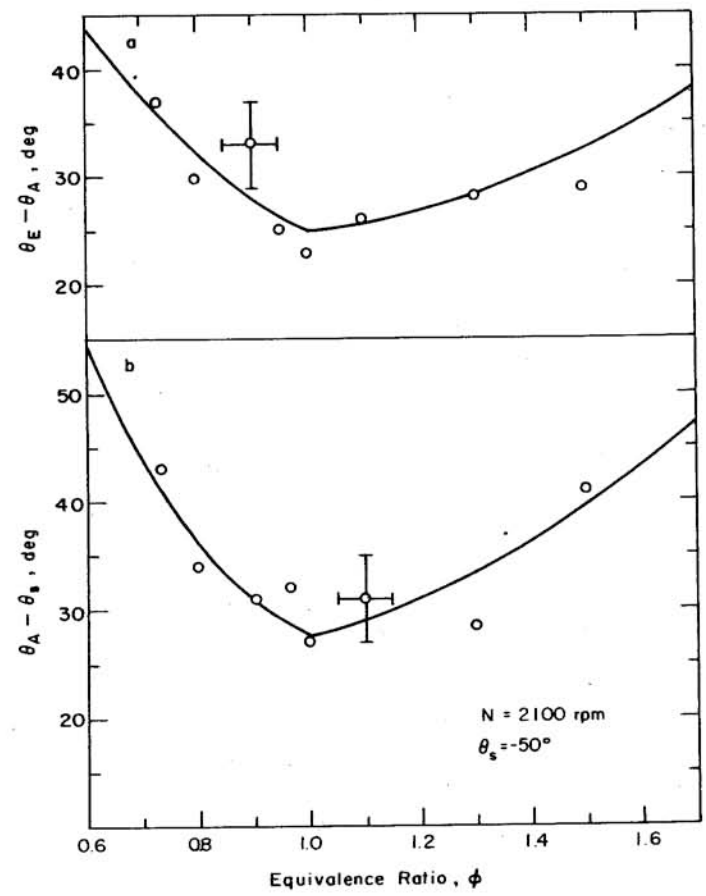

Fig. 12 - Crank angles $\theta_A - \theta_s$ and $\theta_E - \theta_A$ required for flame front to propagate from spark plug to probe A and from probe A to probe E as function of equivalence ratio ϕ for N = 2100 rpm and θ_s = −50. Curves are best fit with theory

$$T_b = (h_{fu} - h_{fb} + c_{pu} T_u)/c_{pb} \quad (84)$$

where c_{pb} and c_{pu} are the effective specific heats for the burned and unburned gases at constant pressure. Using Eqs. 79 and 80 and the relation

$$c_p = c_r + nR \quad (85)$$

we find for $\phi \geqslant 1$

$$T_b = \frac{50000\,(1 - \eta)\,\phi + [8.0 + 0.5\,(\phi - 1)]\,T_u}{12.8 + 4.0\,(\phi - 1)} \quad (86)$$

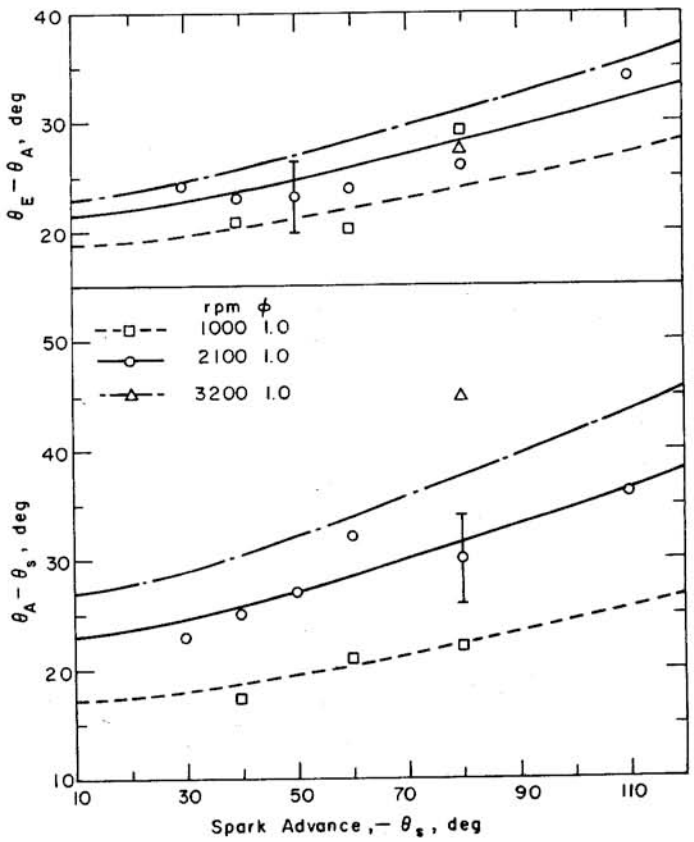

Fig. 13 - Crank angles $\theta_A - \theta_s$ and $\theta_E - \theta_A$ required for flame front to propagate from spark plug to probe A and from probe A to probe E as function of spark advance $-\theta_s$ for $\phi = 1$ and N = 1000, 2100, and 3200 rpm. Curves are best fit with theory

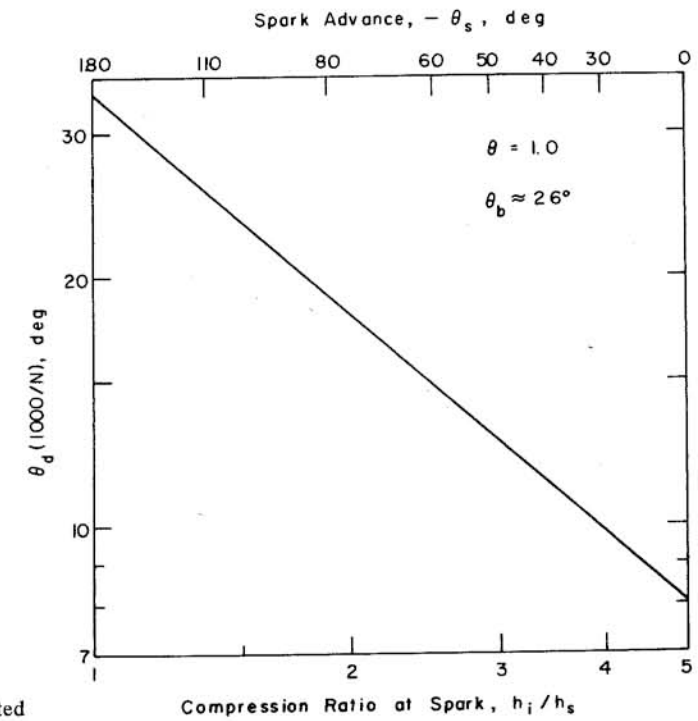

Fig. 14 - Calculated ratio of induction angle to engine speed θ_d/N as function of compression ratio at ignition h_i/h_s for $\phi = 1$. Apparent burning angle θ_b is 26 ± 2 deg for entire range of conditions investigated

and for $\phi \leqslant 1$

$$T_b = \frac{50000\,(1 - \eta) + [8.0 + 0.5\,(\phi - 1)]\,T_u}{12.8 + 4.5\,(\phi - 1)} \qquad (87)$$

where T_b is in R.

The parameters in Eq. 83 may be determined from data on laminar flame speeds summarized by NASA (31). For stoichiometric mixtures of isooctane and air at an initial temperature $T_{u0} = 560$ R and density $\rho/\rho_0 = 1$ atm, we find $u_0 = 860$ in/min, $T_{b0} = 4260$ R and $\alpha = 0.4$. Unfortunately, no sufficiently accurate data could be found from which a determination of E_A could be made. We have therefore chosen E_a to fit the data in Fig. 12B, which gives the dependence of the angle $\theta_A - \theta_s$ on the equivalence ratio. The value so obtained is $E_A = 100{,}000$ Btu/lb mole, which is very reasonable.

Given the laminar flame speed, the data in Figs. 12 and 13 can be used in conjunction with Eqs. 41, 45, and 46 to determine u_e and ℓ_e. Assuming u_e is correlated with the inlet gas speed

$$u_i = \epsilon_v\,(2DL/b^2)\,NS \qquad (88)$$

and ℓ_e with the valve lift L, we obtain

$$u_e = 0.22\,u_i \qquad (89)$$

and

$$\ell_e = 0.17\,(h_s/h_i)L \qquad (90)$$

where the values of b, S, D, and L are given in Table 2 and the volumetric efficiency ϵ_v as a function of engine speed is

N(rpm)	1000	2100	3200
ϵ_v	0.85	0.80	0.70

The factor h_s/h_i in Eq. 90 is the reciprocal of the compression ratio at ignition and was deduced from the correlation. It may be tentatively interpreted as the reduction in the characteristic eddy size due to compression. Although the data indicate that h_s/h_i enters as the first power, the precise exponent depends upon the density dependence of the laminar flame speed, which is rather uncertain at the present time.

The curves in Figs. 10-13 were calculated using the correlations Eqs. 89 and 90 and the corresponding values of the induction angle θ_d and apparent burning angle θ_b are given in Figs. 14 and 15. Note that θ_b varied by less than ±2 deg from a mean value of 26 deg over the entire range of parameters studied, while θ_d varies significantly with all parameters. Although there is considerable scatter in data, due primarily to cycle-to-cycle fluctuation, the overall fit is remarkably good and it is estimated that the correlations are accurate to about ±10%.

SUMMARY AND RECOMMENDATIONS

SUMMARY - A physical model for describing turbulent flame propagation in internal combustion engines has been developed and tested by experiment. The model is based on mixing length theory and contains two parameters: a turbulent entrainment speed u_e and a characteristic eddy radius ℓ_e. Tests of the model have been carried out in a single-cylinder research engine with a bore of 2.5 in for speeds from 1000-

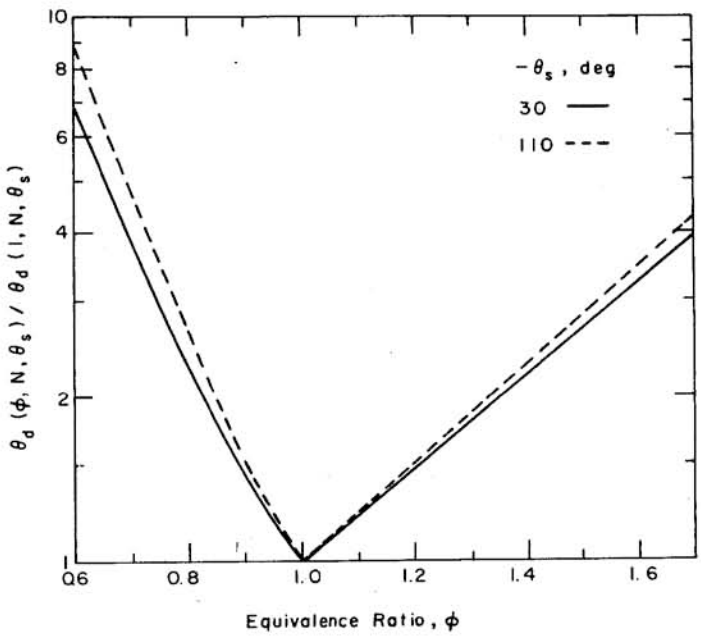

Fig. 15 - Calculated ratio of induction angle $\theta_d\,(\phi, N, \theta_s)$ to induction angle $\theta_d\,(1, N, \theta_s)$ for $\phi = 1$ as function of equivalence ratio ϕ for spark advances $-\theta_s = 30$ and 110 deg

3200 rpm, spark advances from 30-110 deg btc and fuel-air equivalence ratios from 0.7-1.5. The experiments included simultaneous observations of the flame front position and cylinder pressure as functions of the crank angle. The model agrees well with the observations over the entire range of conditions investigated. Correlation formulas given by Eqs. 89 and 90 were developed for determining both u_e and ℓ_e. Using these correlations and the equations developed above, the cylinder pressure, flame radius, and mass fraction of burned gas can be determined as a function of the crank angle from a knowledge of the fundamental engine parameters, fuel type, and operating conditions.

In addition to the burning model, an approximate analytic method for calculating the equilibrium thermodynamic properties of burned gas mixtures over the temperature and pressure ranges of interest for internal combustion engines has also been developed.

RECOMMENDATIONS - Although fairly convincing evidence for the validity of the proposed burning model has been obtained over a wide range of conditions for three of the most important engine parameters (engine speed, spark advance, and equivalence ratio), it would be desirable to check the predictions of the model with regard to numerous other parameters such as fuel type, recycled exhaust fraction, compression ratio, inlet temperature, and engine geometry. In particular, a detailed investigation of the effect of valve lift is needed to verify the assumed correlation (Eq. 89) of u_e with inlet gas speed. Measurements of laminar flame speeds for practical fuels at densities above atmospheric and an investigation of the effect of compression on the turbulence scale are also needed to check further Eq. 90 of ℓ_e with valve lift. Finally, it would be of interest to expand the analysis to include consideration of irregularly shaped chambers, charge stratification, and swirling flows. Such investigations would not only provide a more definitive test of the model, but would also greatly increase its range of practical applications as well. Even in its present form, however, it is anticipated that the model should be useful for design studies aimed at improving the efficiency and pollution characteristics of internal combustion engines.

ACKNOWLEDGMENTS

The authors would like to express their appreciation to the Ford Motor Co. and General Motors Corp. for their financial support of this work. They would like to thank John B. Heywood, Augustus R. Rogvowski, Joseph Rife, Kumihiko Kumiyama, and Richard Vanderpool of M.I.T. for valuable advice and assistance with various parts of this investigation. The assistance of Len Kovachev of General Motors Research Laboratories in detailing the engine head is also gratefully acknowledged.

This work was supported in part by a grant from the Ford Motor Co. and in part by a grant-in-aid award to Norman Blizard by the General Motors Corp.

REFERENCES

1. J. B. Heywood, et al., "Prediction of Nitric Oxide Concentrations in a Spark Ignition Engine Compared with Exhaust Measurements." Paper 710011 presented at Automotive Engineering Congress, Detroit, January 1971.

2. L. J. Spadiccini and W. Chinitz, "An Investigation of Nonequilibrium Effects in an Internal Combustion Engine." ASME paper 71-WA/Fu2, Nov. 28, 1971.

3. A. S. Sokolik, ed., "Turbulent Combustion in an Engine Cylinder." Self-Ignition Flame and Detonation in Gases, 1963, p. 284 ff.

4. Daniell, Proc. Roy. Soc., London, A126, 1930, p. 393.

5. G. A. Lavoie, "Spectroscopic Measurements of Nitric Oxide in an S. I. Engine." Comb. and Flame, Vol. 15 (1970), p. 97 ff.

6. G. A. Lavoie, J. B. Heywood, and J. C. Keck, "Experimental and Theoretical Study of Nitric Oxide Formation in Internal Combustion Engines." Comb. Sci. and Tech., Vol. 1 (1970), p. 313.

7. Lewis and Von Elbe, "Combustion, Flames, and Explosions of Gases." Cambridge University Press, 1938, p. 211.

8. W. A. Sirignano, "One-Dim. Anal. of Comb. in S. I. Engine." Guggenheim Laboratories, Princeton, N. J., 1972.

9. A. H. Rasegan, "The Effect of Turbulence on Combustion in a Spark-Ignited I. C. Engine." S. M. Thesis, M.I.T., August 1965.

10. Clark, W. A. Bone, and Townend, "Flame and Combustion in Gases." 1927, p. 244 ff.

11. Semenov and Clark, "A Study of Turbulent Gas Motion in the Cylinder of a Piston Engine." Sbornik Gorenie v Turbulentnom potoke, Moskus, Izdatel'stvo Akademie Nauk SSR, 1959, pp. 141-167.

12. C. L. Bouchard, et al., "Altitude and Other Variables Affecting Flame Speed in the Otto Cycle Engine." SAE Transactions, Vol. 32 (1937).

13. A. R. Rogowski, "Elements of Internal Combustion Engines." Chs. 2-4, 1965.

14. H. C. Hottel, et al., "Thermodynamic Charts." New York: John Wiley Co., 1949.

15. JANAF Thermochemical Tables, Dow Chemical Co., distributed by Clearinghouse.

16. C. F. Taylor and E. S. Taylor, "The Internal Combustion Engine." Scranton, Pa.: International Textbook Co., 1966.

17. C. F. Taylor, "The I. C. Engine in Theory and Practice." Cambridge: M.I.T. Press, 1971, Vol. II, p. 612, Vol. I, pp. 114-118.

18. S. Curry, "Effect of Antiknocks on Flame Propagation in a Spark Ignition Engine." 9th Symp. Comb., 1962, p. 1056 ff.

19. S. Curry, "Three Dimensional Study of Flame Propagation in a Spark Ignition Engine." SAE Transactions, Vol. 71 (1963), paper 452-B.

20. D. A. Hirschler, et al., "Deposit Induced Ignition, Evaluation in a Laboratory Engine." SAE Transactions, Vol. 62 (1954).

21. S. Kumagai and Y. Kudo, "Flame Studies by Means of Ionization Gaps in a High Speed Spark Ignition Engine." 9th Symp. Comb., p. 1069 et seq. 1958, p. 1069 ff.

22. J. A. Robinson, et al., "Investigating Rumble in Single Cylinder Engines." SAE Transactions, Vol. 66 (1959), paper 61-H.

23. K. Schnauffer, "Engine-Cylinder Flame Propagation Studied by New Methods." SAE Transactions, Vol. 29 (1934).

24. J. A. Warren and J. B. Hinkamp, "New Instrumentation for Engine Combustion Studies." SAE Transactions, Vol. 64 (1956).

25. H. F. Calcote, "Ion Production and Recombination in Flames." 8th Symposium (Int'l.) on Combustion, 1960, p. 184 ff.

26. H. F. Calcote, "Ion and Electron Profiles in Flames." Combustion and Flame, Vol. 1 (1957), p. 385 ff.

27. H. F. Calcote and J. King, "Ionization in Flames with Langmuir Probes." 8th Symp. Comb., 1960, p. 434 ff.

28. Sanborn C. Brown, "Basic Data of Plasma Physics." New York: M.I.T. Press and John Wiley and Sons, 1959.

29. R. A. Strehlow, "Fundamentals of Combustion." 1963, p. 205.

30. F. A. Williams, "Combustion Theory." Chs. 5-8, 1964.

31. NASA Report 1300, "Basic Considerations in the Combustion of Hydrocarbon Fuels with Air." Prepared by Propulsion Chemistry Division, Lewis Flight Center, 1957.

Society of Automotive Engineers, Inc.
TWO PENNSYLVANIA PLAZA, NEW YORK, N.Y. 10001

20 page booklet.

Printed in U.S.A.